

A kinematic wave theory of lane-changing traffic flow

Wen-Long Jin *

September 13, 2018

Abstract

Frequent lane-changes in highway merging, diverging, and weaving areas could disrupt traffic flow and, even worse, lead to accidents. In this paper, we propose a simple model for studying bottleneck effects of lane-changing traffic and aggregate traffic dynamics of a roadway with lane-changing areas. Based on the observation that, when changing its lane, a vehicle affects traffic on both its current and target lanes, we propose to capture such lateral interactions by introducing a new lane-changing intensity variable. With a modified fundamental diagram, we are able to study the impacts of lane-changing traffic on overall traffic flow. In addition, the corresponding traffic dynamics can be described with a simple kinematic wave model. For a location-dependent lane-changing intensity variable, we discuss kinematic wave solutions of the Riemann problem of the new model and introduce a supply-demand method for its numerical solutions. With both theoretical and empirical analysis, we demonstrate that lane-changes could have significant bottleneck effects on overall traffic flow. In the future, we will be interested in studying lane-changing intensities for different road geometries, locations, on-ramp/off-ramp flows, as well as traffic conditions. The new modeling framework could be helpful for developing

*Department of Civil and Environmental Engineering, California Institute for Telecommunications and Information Technology, Institute of Transportation Studies, University of California, Irvine, CA 92697-3600. Tel: 949-824-1672. Fax: 949-824-8385. E-mail: wjin@uci.edu. Author for correspondence

ramp metering and other lane management strategies to mitigate the bottleneck effects of lane-changes.

Keywords: LWR model, fundamental diagram, lane-changing intensity variable, Riemann problem, kinematic waves, supply-demand method, bottleneck effects, NGSIM data

1 Introduction

An understanding of the evolution of traffic dynamics is the foundation of transportation network analysis, management, control, and planning. In the celebrated LWR model (Lighthill and Whitham, 1955; Richards, 1956), vehicular traffic is viewed as a continuous fluid flow, and traffic dynamics are described by the changes in (x, t) -space of three aggregate variables: density ρ , speed v , and flow-rate q . The model is can be written as

$$\frac{\partial \rho}{\partial t} + \frac{\partial \rho V(\rho)}{\partial x} = 0, \quad (1)$$

which is based on three assumptions:

- The fundamental law of traffic flow:

$$q = \rho v, \quad (2)$$

- Traffic conservation

$$\frac{\partial \rho}{\partial t} + \frac{\partial q}{\partial x} = 0, \quad (3)$$

- Fundamental diagram of speed-density relationship

$$v = V(\rho). \quad (4)$$

The first two assumptions can be derived from the continuum assumption of traffic flow (Haberman, 1977, Chapters 59, 60). An equilibrium speed-density relationship assumption (4) has been shown

to be valid in stationary states (Del Castillo and Benitez, 1995). Such a relationship can also be derived from various car-following models in steady states (Gazis et al., 1961) and (Haberman, 1977, Chapter 61). In this sense, the speed-density relationship in (4) captures the longitudinal interactions among vehicles, and the traditional LWR model is consistent with car-following behaviors at the aggregate level (Newell, 1961). In the LWR model, traffic dynamics are described by combinations of shock and rarefaction waves (Whitham, 1974), and the LWR model is thus called the kinematic wave model of traffic flow.

Major roadways, however, usually have multiple lanes, and vehicles can not only change speeds, but also change lanes. That is, vehicles can have both longitudinal and lateral movements. A lane-changing area is a region, where one or more streams of vehicles systematically change their lanes. Such areas can be near a merging junction and lane-drops, upstream to a diverging junction, inside a weaving section, or around a cloverleaf interchange (Milam and Choa, 1998; Cassidy and Rudjanakanoknad, 2005). Since bottlenecks (Hall and Agyemang-Duah, 1991) and accidents (e.g. Golob et al., 2004) tend to occur in these areas, it is important to understand phenomena associated with lane-changing traffic. In this study, we assume that different lanes are balanced on average; i.e., vehicle speeds are the same across different lanes at the same location and time. In reality, it has been observed that traffic is nearly balanced inside major weaves, where speed difference for weaving and non-weaving vehicles is not statistically significant (about 5 mph) (Roess et al., 1974). Actually, imbalance among different lanes is usually a reason for lane-changing, and lane-changing traffic can have balancing effect; i.e., under certain situations, lane-changes could smooth out differences between lanes, and the balancing effect could be beneficial to the whole traffic system in achieving higher capacity.

At the microscopic level, vehicles' speed adjustment behaviors have been modeled by car-following models (Gazis et al., 1961); similarly, lane-choice behaviors on why, when, where, and

how a vehicle changes its lane are modeled by lane-changing models (Gipps, 1986; Yang, 1997; Toledo et al., 2003; Kesting et al., 2007). These models can describe detailed lane-changing behaviors, but usually contain a large number of parameters and cannot provide intuitive descriptions of system-level effects of lane-changing traffic. At the macroscopic level, many studies have been carried out to understand various characteristics of lane-changing traffic, including exchange of flows between lanes (Michalopoulos et al., 1984; Holland and Woods, 1997; Daganzo, 2002; Coifman, 2003), density oscillation and instability issues (Gazis et al., 1962; Munjal and Pipes, 1971), and the degree of First-In-First-Out violation among vehicles (Jin et al., 2006). In particular, characteristics of weaving sections have been extensively studied since the publication of Highway Capacity Manual in 1950, and many methods have been proposed to analyze levels of service at weaving areas, usually measured by speeds of weaving and non-weaving vehicles (e.g. Leisch, 1979). In these methods, parameters include weave type, geometric configurations, the number of lanes, the length of a weaving area, weaving flow, non-weaving flow, and the number of lane-changes. In (Cassidy et al., 1989; Cassidy and May, 1991; Ostrom et al., 1993; Windover and May, 1994), the distribution of weaving and non-weaving traffic on rightmost lanes was also studied for different locations. Eads et al. (2000) proposed a framework for evaluating dynamic capacities of a weaving section. In (Laval and Daganzo, 2006), a hybrid model of lane-changing traffic was proposed, and it was shown that systematic lane-changes could cause a capacity-drop consistent with observations. All these studies, however, do not provide a simple approach for analyzing the impacts of lane-changing traffic and the corresponding traffic dynamics at the aggregate level.

In this paper, we attempt to fill this gap and develop a simple kinematic wave model of lane-changing traffic. Based on the observation that, when changing its lane, a vehicle is the leader of two following vehicles on its current and target lanes, we modify the speed-density relationship in (4) by adding an effective additional density, equal to total density of all lanes times a lane-changing

intensity variable (or simply intensity) $\epsilon(x, t)$. With the new fundamental diagram for both car-following and lane-changing traffic, we then introduce a kinematic wave model based on the LWR model. When the lane-changing intensity is location-dependent, we analyze the new kinematic wave model as a system of hyperbolic conservation laws. We also calibrate a relationship between lane-changing intensity and traffic density with observed vehicle trajectories in a weaving section. Note that lane-changing intensity $\epsilon(x, t)$ is determined by drivers' lane-changing choices and characteristics in a road section during a time interval. Therefore, $\epsilon(x, t)$ is highly related to the location in a lane-changing section, on-ramp and off-ramp flows, and roads' geometric configurations. In this paper, we demonstrate that, once $\epsilon(x, t)$ is known, we are able to evaluate the impacts of lane-changing traffic at the aggregate level within the framework of kinematic waves.

The rest of the paper is organized as follows. In Section 2, we introduce a lane-changing intensity variable, a modified fundamental diagram, and a kinematic wave model for lane-changing traffic. In Section 3, we analyze the kinematic wave model as a nonlinear resonant system and propose a corresponding supply-demand method for numerical solutions. In Section 4, we calibrate a relationship between the lane-changing intensity variable and traffic density for a weaving section with NGSIM data. Finally, some implications and extensions of this study are discussed.

2 A kinematic wave model of lane-changing traffic

2.1 Model derivation

Assume the longitudinal axis is x , and the lateral axis is y . Then the movement of a lane-changing vehicle can be represented by a trajectory in (x, y, t) space. As shown in Figure 1, during a time period of Δt , a lane-changing vehicle can move Δx and Δy in the x and y directions, respectively. We can see that the lateral displacement threshold of the lane-changing vehicle, or simply lane-changing

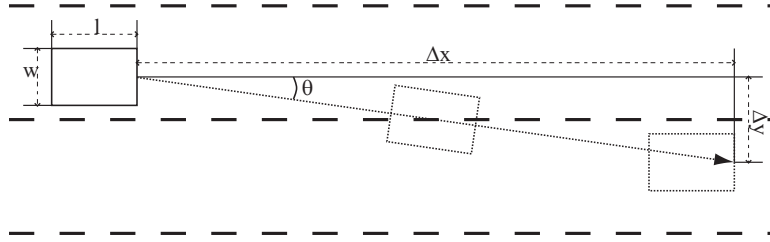


Figure 1: An illustration of a lane-change

threshold, Δy , should be at least the width of the vehicle w . To accomplish a lane-change, a vehicle first usually signals its intention. In very sparse traffic, it can easily find a gap big enough to switch to its target lane without waiting too long or interrupting traffic stream on either its current or target lanes. However, in congested traffic, it usually has to slow down first and wait for a gap or speed up to squeeze in. In this process, following vehicles on its current lane have to maneuver accordingly, and following vehicles on the target lane may slow down or switch to other lanes to let it in. That is, a lane-changing vehicle has longitudinal influence on its current lane and lateral influence on its subject lane. In a lane-changing area, individual vehicles' lane-changing choices may vary significantly (Gipps, 1986), but our experience and many studies suggest that systematic lane-changing vehicles may disrupt traffic flow.

Since (Greenshields, 1935), speed- or flow-rate-density relations, $v = V(\rho)$ and $q = \rho V(\rho)$ respectively, have been used to capture drivers' response to traffic environment at the aggregate level. Note that, traffic density ρ is traditionally defined as the number of vehicles per unit length of road. Thus traditional fundamental diagram captures only longitudinal interactions between vehicles when they follow each other, but not lateral interactions when they change lanes. Therefore, the traditional LWR model cannot be directly applied to describe traffic dynamics in lane-changing areas.

Since a vehicle uses both its current and target lanes during a lane-change, we propose to double

the contribution of a lane-changing vehicle to total density. I.e., lane-changing traffic causes effective additional density. If denoting a lane-changing intensity variable, $\epsilon(x, t)$, the effective total traffic density is given by

$$\bar{\rho}(x, t) = \rho(x, t)(1 + \epsilon(x, t)). \quad (5)$$

Furthermore, for lane-changing traffic, we use the following modified speed-density relationship:

$$v = V(\bar{\rho}) = V(\rho(1 + \epsilon)). \quad (6)$$

Then, the fundamental diagram with lane-changing effect is

$$q = \rho V((1 + \epsilon)\rho). \quad (7)$$

Correspondingly, the fundamental diagram without lane-changing effect is

$$q = \bar{\rho} V(\bar{\rho}) = (1 + \epsilon)\rho V((1 + \epsilon)\rho). \quad (8)$$

By comparing (8) and (7), we will be able to understand the impact of lane-changing traffic.

With the fundamental diagram incorporating lane-changing intensity, we can model lane-changing traffic dynamics in the framework of kinematic wave theories as follows:

$$\rho_t + (\rho V(\rho(1 + \epsilon)))_x = 0, \quad (9)$$

which can be considered as an extension of the LWR model for equilibrium lane-changing traffic.

2.2 Determination of lane-changing intensity in uniform traffic

Generally $\epsilon(x, t)$ is time- and location-dependent, and $\epsilon(x, t) \geq 0$ due to the bottleneck effect. Since $\frac{\partial V}{\partial \epsilon} = V'\rho$, which is negative in general, this modified speed-density relationship is consistent with observations (Fazio and Rouphail, 1986) that the total number of lane-shifts in a weaving section, proportional to ϵ , is negatively correlated to weaving and non-weaving speed. At the microscopic

level, lane-changing intensity $\epsilon(x, t)$ is determined by drivers' lane-changing choices and characteristics in a road section during a time interval. At the macroscopic level, the lane-changing intensity variable in (5) are related to locations, road geometric configurations, on-ramp and off-ramp flows, and other traffic conditions. Therefore, in practical applications, $\epsilon(x, t)$ has to be calibrated for different locations of a lane-changing area and traffic conditions.

Here we attempt to determine lane-changing intensity when traffic conditions are uniform in the lane-changing region; i.e., traffic density is the same across the region and for all lanes, and all vehicles travel at the same speed. This is not meant to provide a generic formula for computing ϵ in (5). Instead, we intend to show which parameters could affect the lane-changing effect at the aggregate level.

For a lane-changing section of length L , we have the following quantities: ρ_{LC} is the density of lane-changing traffic, ρ_{NLC} the density of non-lane-changing traffic, $\rho = \rho_{LC} + \rho_{NLC}$ the total density, v the speed of both lane-changing and non-lane-changing vehicles, $q_{LC} = \rho_{LC}v$ the flow-rate of lane-changing traffic, and $q_{NLC} = \rho_{NLC}v$ the flow-rate of non-lane-changing traffic. Then, the time for all vehicles to traverse the lane-changing region is $T = L/v$. In order to understand how much effect lane-changing traffic can have on total traffic, we have to know the time for finishing a lane-changing maneuver and the number of lane-changes.

We denote the total number of lane-changes in the lane-changing area during a period of T by N_{LC} . In literature, the lane-changing frequencies have been studied for different traffic conditions and road geometric configurations (Worrall and Bullen, 1970; Worrall et al., 1970; Pahl, 1972; Chang and Kao, 1991; Klar and Wegener, 1999). Here, we are mostly interested in the relationship between lane-changing traffic flow and the number of lane-changes for relatively congested traffic. In (Fazio and Rouphail, 1986), it has been calibrated that the total number of lane-changes are linear to weaving, i.e., lane-changing, flows for different lane configurations of

weaving areas. In (Fitzpatrick and Nowlin, 1996), it is observed that a weaving vehicle generally takes 1.33 lane-changes in one-sided weaving operations on one-way frontage roads. Thus here we simply assume a linear relationship between the number of lane-changes and lane-changing flow; i.e., $N_{LC} = \alpha q_{LC} T = \alpha \rho_{LC} L$, where the coefficient α , the average number of lane-changes of each lane-changing vehicle, could be related to lane-configurations, number of lanes, traffic conditions, drivers' tendency to lane-changing, and the length of the section. In addition, α could also depend on location (Cassidy and May, 1991; Windover and May, 1994).

We denote lane-change duration by t_{LC} , which starts when a vehicle signals its lane-changing intention and ends when it finishes a lane-change. If the width of a lane is D , and the average lane-changing angle θ , we then have

$$t_{LC} = \frac{D}{v \tan \theta}. \quad (10)$$

Note that θ is related to drivers' behavior, road geometric configurations, and traffic conditions. Usually the time to complete a lane-changing maneuver is around 2.5 sec on freeways (Wang and Prevedouros, 1998), while about 10 sec on surface streets (Sheu and Ritchie, 2001).

Therefore, by doubling the number of lane-changing vehicles during their lane-changing periods, the effective number of vehicles at any moment is

$$\bar{N} = \frac{\rho L T + N_{LC} t_{LC}}{T} = \rho L + \alpha \rho_{LC} L \frac{t_{LC}}{T}. \quad (11)$$

Then we can obtain the lane-changing intensity variable, ϵ , in (5) as

$$\epsilon = \frac{N_{LC} t_{LC}}{\rho L T} = \frac{N_{LC} t_{LC}}{N T} = \alpha \frac{\rho_{LC} t_{LC}}{\rho T}. \quad (12)$$

In this sense, the lane-changing intensity can be considered as ratio of the total lane-changing time to the total traveling time during a time interval on a road section. As expected, lane-changing intensity variable is determined by the number of lane-changes, the lane-changing duration, and

traffic density in the lane-changing area. In particular, α and ρ_{LC} or N_{LC} can depend on road geometry, locations, and traffic conditions.

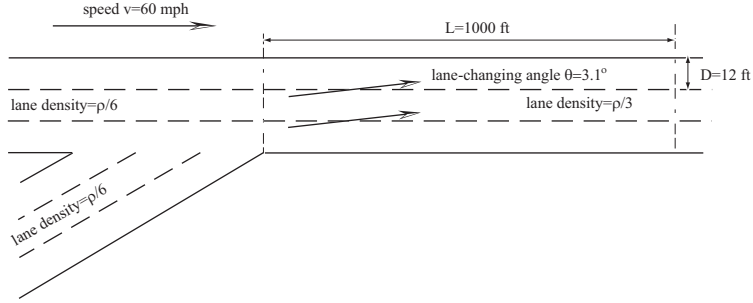


Figure 2: A lane-changing area downstream to a merging junction

As a simple example, we consider a uniform, three-lane lane-changing region, which is downstream to a merging junction connecting two three-lane roads as shown in Figure 2 ¹. The length of the lane-changing area is $L = 1000$ ft, the width of a lane $D = 12$ ft, and both branches have the same density of $\rho/2$; i.e., traffic density on each lane is $\rho/6$ before merging. We assume that all lanes in the lane-changing region are fully balanced; i.e., traffic density on each lane in this region is twice as that before merging, $\rho/3$. Therefore, one third of vehicles from the merging branch, i.e., $\rho/6$, have to stay on the rightmost lane in the lane-changing region with no lane-change, one third will change one lane to the middle lane, and one third will change two lanes to the leftmost lane. In this case, the total density in the lane-changing region is ρ , and the density of lane-changing traffic is that from the merging branch; i.e., $\rho_{LC} = \rho/3$. Then we have the average number of lane-changes of a merging vehicle

$$\alpha = \frac{\rho/6 \cdot 0 + \rho/6 \cdot 1 + \rho/6 \cdot 2}{\rho/3} = 1.5.$$

If we assume that vehicle speed $v = 60$ mph and the lane-change duration $t_{LC} = 2.5$ sec, then the

¹Here we simplify the problem by assuming that all lane-changes occur in the region downstream to the merging junction. In reality, some vehicles might change their lanes upstream to the merging junction.

time for a vehicle to traverse the lane-changing region is $T = L/v=11.4$ sec, and we can find from (10) that the lane-changing angle $\theta = 3.1$ degrees. Then from (12), we can have

$$N_{LC}t_{LC} = \frac{\rho}{6}Lt_{LC} + \frac{\rho}{6}L2t_{LC} = \frac{\rho}{2}Lt_{LC},$$

and the lane-changing intensity variable in (12) is

$$\epsilon = \frac{1}{2} \frac{2.5}{11.4} = 0.11.$$

Here we assume that lane-changes are evenly distributed over the whole road section. In reality, however, the distribution may be uneven, and we may have a location-dependent lane-changing intensity variable $\epsilon(x)$.

2.3 Bottleneck effects of lane-changing traffic

We consider the following triangular fundamental diagram (Munjal et al., 1971; Haberman, 1977; Newell, 1993),

$$V(\rho) = \begin{cases} v_f, & 0 \leq \rho \leq \rho_c; \\ \frac{\rho_c}{\rho_j - \rho_c} v_f \frac{\rho_j - \rho}{\rho}, & \rho_c < \rho \leq \rho_j, \end{cases}$$

$$Q(\rho) = \begin{cases} v_f \rho, & 0 \leq \rho \leq \rho_c; \\ \frac{\rho_c}{\rho_j - \rho_c} v_f (\rho_j - \rho), & \rho_c < \rho \leq \rho_j, \end{cases}$$

where v_f is the free flow speed, ρ_j the jam density, and ρ_c the critical density where flow-rate, $q = \rho v$, attains its maximum, i.e. the capacity. The values of these parameters are: $v_f = 65$ mph, $\rho_j = 240$ vpmpl, $\rho_c = \rho_j/6 = 40$ vpmpl, and the capacity is $Q_{max} = 2600$ vphpl (Del Castillo and Benitez, 1995). After introducing lane-changing effect, we then have the following fundamental diagram,

$$V(\epsilon, \rho) = \begin{cases} v_f, & 0 \leq \rho \leq \rho_c/(1 + \epsilon); \\ \frac{\rho_c}{\rho_j - \rho_c} v_f \frac{\rho_j - \rho(1 + \epsilon)}{\rho(1 + \epsilon)}, & \rho_c/(1 + \epsilon) < \rho \leq \rho_j/(1 + \epsilon), \end{cases} \quad (13)$$

$$Q(\epsilon, \rho) = \begin{cases} v_f \rho, & 0 \leq \rho \leq \rho_c / (1 + \epsilon); \\ \frac{\rho_c}{\rho_j - \rho_c} v_f \frac{\rho_j - \rho(1 + \epsilon)}{1 + \epsilon}, & \rho_c / (1 + \epsilon) < \rho \leq \rho_j / (1 + \epsilon). \end{cases} \quad (14)$$

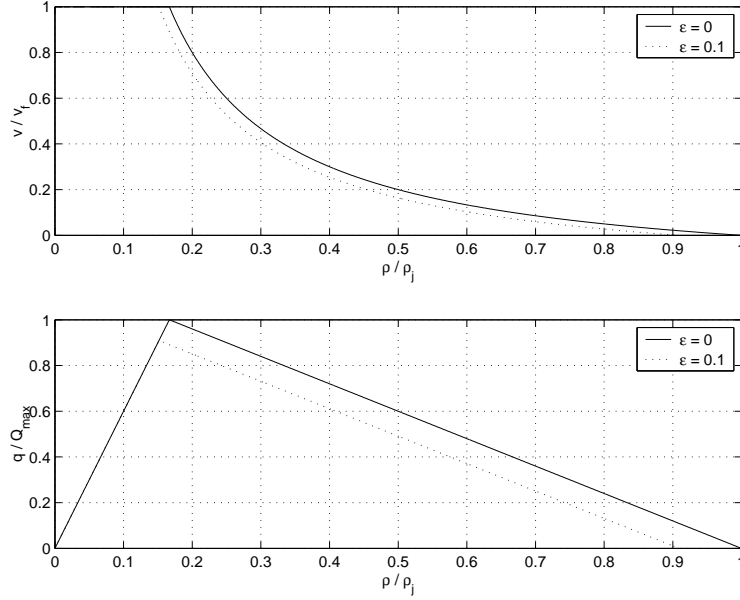


Figure 3: The triangular fundamental diagram with constant lane-changing effect

For one example, we assume constant lane-changing effect, $\epsilon = 0.1$. The relationships between the standardized density, speed, and flow-rate are shown in Figure 3. From the figure, we can see that: (i) lateral interactions can be omitted when traffic is relative sparse; (ii) there exists capacity reduction of $1 - 1/1.1=9.1\%$, which is consistent in magnitude with observations in (Cassidy and Bertini, 1999)²; and (iii) the observed jam density is lower than maximum jam density, which could be one reason of observing different jam densities (Del Castillo and Benitez, 1995). That is, for the same road section, constant lane-changes can yield a lower throughput. This clearly demonstrates the bottleneck effect of lane-changing traffic.

For another example, we consider the following density-dependent lane-changing effect, which

²Note that reasons of bottleneck were not discussed in this study, and we suspect that systematic lane-changes caused by merging traffic from on-ramps could have significant contributions.

has a jump at critical density,

$$\epsilon(\rho) = \begin{cases} 0, & \rho < \rho_c; \\ \frac{2-2\rho/\rho_j}{15+2\rho/\rho_j}, & \rho \geq \rho_c. \end{cases} \quad (15)$$

As shown in Figure 4, the lane-changing effect is approximately linear for congested traffic, and the resulted fundamental diagram has a shape of reverse- λ (Koshi et al., 1983). Since lane-changing intensity is related to the location, road geometry, on-ramp and off-ramp flows, and other exogenous conditions, it is possible to have a discontinuous $\rho - \epsilon$ relationship. In (Cassidy and Rudjanakanoknad, 2005), for example, it was observed that lane-changing intensity is significantly higher when a 16-vehicle queue appears on the shoulder lane. Therefore, this discontinuous $\rho - \epsilon$ relationship could also be a cause of capacity-drop: when traffic density increases over a critical value, the number of lane-changes significantly increases, and the overall capacity drops as a result.

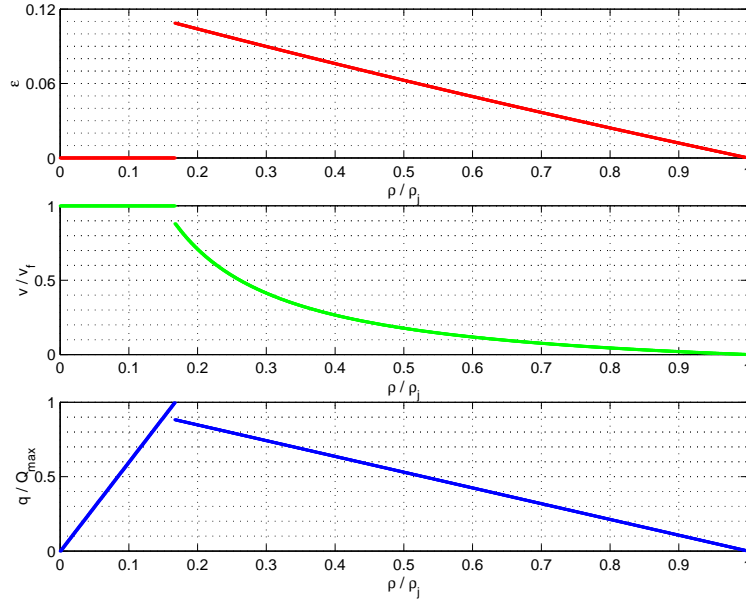


Figure 4: A fundamental diagram of reverse- λ shape with density-dependent lane-changing effect

3 Traffic dynamics for location-dependent lane-changing intensities

In this section, we consider a special case, where the lane-changing intensity variable, $\epsilon(x, t)$, is independent of traffic conditions and only a function of location denoted by $\epsilon(x)$. Although simplified, this assumption does capture the most pronounced feature that lane-changing intensity is location-dependent. For this scenario, we can analyze (9) and understand some fundamental traffic dynamics in lane-changing areas. In the literature, there have been many methods for analyzing such an inhomogeneous LWR model with discontinuous flux functions (refer to (Jin et al., 2009) for a survey). In this study, we follow an approach proposed in (Jin and Zhang, 2003).

3.1 A system of hyperbolic conservation laws

For a location dependent lane-changing intensity $\epsilon(x)$, we obtain a simple conservation law of lane-changing coefficient,

$$\epsilon_t = 0, \tag{16}$$

which is equivalent to saying that ϵ is time-independent.

Without considering inhomogeneities of links (Jin and Zhang, 2003) or merging and diverging effect, we can have the following system of conservation laws,

$$U_t + F(U)_x = 0, \tag{17}$$

where $U = (\epsilon, \rho)$, $F(U) = (0, Q(\epsilon, \rho))$, $x \in R$, and $t \geq 0$. Note that the domains of ϵ and ρ are $\epsilon \in [0, \infty)$ and $\rho \in [0, \frac{\rho_j}{1+\epsilon}]$ respectively.

Here we use a differentiable, concave fundamental diagram in our analysis. For example, we

can use the following maximum sensitivity model (Del Castillo and Benitez, 1995):

$$V(\rho) = v_f \left\{ 1 - \exp \left[1 - \exp \left(\frac{|c_j|}{v_f} \left(\frac{\rho_j}{\rho} - 1 \right) \right) \right] \right\}, \quad (18)$$

where c_j is the shock wave speed for jammed traffic. In this fundamental diagram, $V' < 0$ and $\frac{d^2}{d\rho^2}Q(\rho) < 0$.

For the kinematic wave model of lane-changing traffic, (17), the second term of flux, $F(U)_x$, can be linearized as $\partial F(U)U_x$ with

$$\partial F = \begin{bmatrix} 0 & 0 \\ \rho^2 V' & V + \rho(1 + \epsilon)V' \end{bmatrix},$$

whose two eigenvalues, or wave speeds, are $\lambda_0(U) = 0$, and $\lambda_1(U) = V + \rho\epsilon V' = Q'((1 + \epsilon)\rho)$.³ The corresponding eigenvectors are

$$\vec{R}_0 = \begin{bmatrix} V + \rho(1 + \epsilon)V' \\ -\rho^2 V' \end{bmatrix}, \quad \vec{R}_1 = \begin{bmatrix} 0 \\ 1 \end{bmatrix}.$$

Since $V \geq 0$ and $V' < 0$, it is possible that $\lambda_1 = 0 = \lambda_0$. Therefore, (17) is a non-strictly hyperbolic system.

In addition, if defining the critical traffic state $U_* = (\epsilon_*, \rho_*)$ by $\lambda_1(U_*) = 0$, we then have the following results. First,

$$\frac{\partial}{\partial \rho} \lambda_1(U_*) = \frac{\partial^2 Q}{\partial \rho^2} |_{U_*} = (1 + \epsilon)Q''((1 + \epsilon)\rho) |_{U_*} < 0, \quad (19)$$

since Q is strictly concave in $(1 + \epsilon)\rho$. Second,

$$\frac{\partial}{\partial \epsilon} Q(U_*) = \rho^2 V' |_{U_*} \leq 0.$$

From (19), the wave speed λ_1 is decreasing with respect to traffic density. In addition, $\lambda_1(\epsilon, \rho = 0) = v_f > 0$ and $\lambda_1(\epsilon, \rho) = \epsilon \rho V' < 0$ when $(1 + \epsilon)\rho = \rho_j$. Therefore, for any weaving factor ϵ_* ,

³By assuming $\bar{\rho} = \rho/(1 + \epsilon)$, we have that $Q = \frac{1}{1 + \epsilon} \bar{\rho} V(\bar{\rho}) = \frac{1}{1 + \epsilon} Q(\bar{\rho})$ and $\lambda_1(U) = \frac{\partial Q}{\partial \rho} = \frac{1}{1 + \epsilon} \frac{dQ}{d\bar{\rho}} \frac{\partial \bar{\rho}}{\partial \rho}$. Therefore, $\lambda_1(U) = \frac{dQ}{d\bar{\rho}} = Q'((1 + \epsilon)\rho)$.

we can find a unique critical state $U_* = (\epsilon_*, \rho_*)$. Further, since $\partial\lambda_1/\partial\rho < 0$, $Q(U_*)$ is indeed the maximum flow-rate for ϵ_* and equals $\frac{1}{1+\epsilon_*} \max\{Q(\epsilon, \rho)|\epsilon = 0\}$, where $\max\{Q(\epsilon, \rho)|\epsilon = 0\}$ is the capacity without lane-changes, and $\frac{1}{1+\epsilon_*}$ reflects capacity-drop caused by lane-changes. Here we call $\rho_* = \Gamma(\epsilon_*)$ as the transitional curve, since traffic states on its left side are under-critical (UC) while those on its right side are over-critical (OC). From these properties, (17) is a nonlinear resonant system and, in the neighborhood of a critical state, the Riemann problem can be uniquely solved (Isaacson and Temple, 1992).

3.2 Solutions of the Riemann problem

We consider the Riemann problem of (17) with the following initial conditions,

$$U(x, t = 0) = \begin{cases} U_L, & x < 0, \\ U_R, & x > 0, \end{cases}$$

where $U_L = (\epsilon_L, \rho_L)$ and $U_R = (\epsilon_R, \rho_R)$. Since, in the Godunov method (Godunov, 1959), general initial conditions can be approximated by piece-wisely linear functions, we can solve the Riemann problem at each boundary to find the flux and then update traffic conditions for the next time step.

According to (Isaacson and Temple, 1992), the Riemann problem is solved by a combination of two basic types of waves, which are associated with the two eigenvalues of ∂F : we have 0- or standing waves with wave speed $\lambda_0 = 0$, and 1-waves with wave speed λ_1 . Note that 0-waves carry contact discontinuities, and 1-waves include traditional shock and rarefaction waves. In the $\rho - \epsilon$ phase plane, (U_L, U_R) yielding 0-waves forms a 0-curve, and similarly we can define a 1-curve. Further, 0-curves are the integral curves of eigenvector \vec{R}_0 , and 1-curves are those of \vec{R}_1 . They are $\rho V(\rho(1 + \epsilon)) = \text{const}$ and $\epsilon = \text{const}$, respectively. A 0-curve, a 1-curve, and the transitional curve are shown in Figure 5. For a Riemann problem, its solutions must satisfy both Lax's (Lax, 1972) and Isaacson and Temple's (Isaacson and Temple, 1992) entropy conditions, such that resulted waves

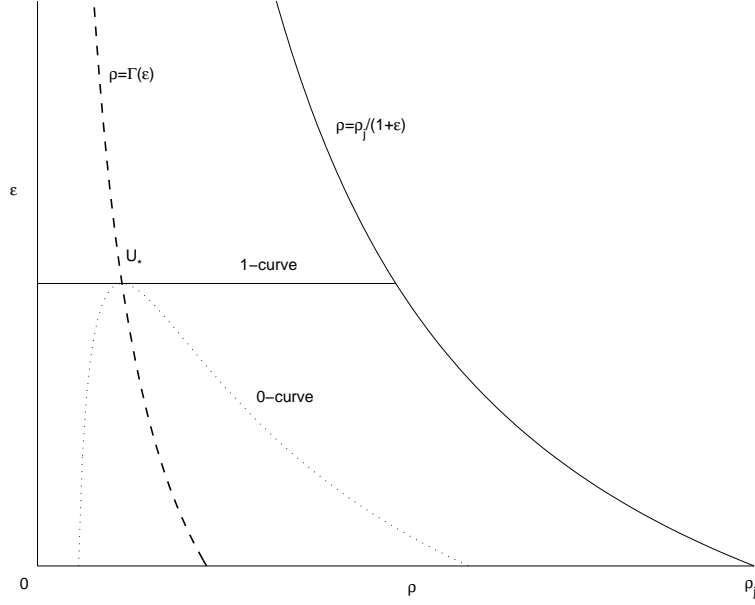


Figure 5: A 0-curve, 1-curve, and the transitional curve in (ρ, ϵ) -plane

increase their wave speeds from left to right, and 0-curves do not cross the transitional curve. Since both 0- and 1-waves are linear in the sense that $U(x, t) = U(x/t)$, then from the Riemann solutions, we can obtain the boundary flux through $x = 0$ as $q = Q(U(x = 0, t > 0))$.

As shown in Figure 6, when U_L is UC, i.e. to the left of the transitional curve in the phase plane, we have $\rho_L \leq \Gamma(\epsilon_L)$ and can divide the $\rho - \epsilon$ phase plane into four regions by the thick curves and obtain the four types of wave solutions for different values of U_R , which satisfy the two aforementioned entropy conditions. Here kinematic wave solutions of Type 1 are carefully explained, and solutions of Types 2 to 4 are given in Appendix.

Type 1 When U_R is in Region 1, $\rho_R \leq \Gamma(\epsilon_R)$, $Q(U_R) \leq Q(U_L)$, and $Q(\epsilon_R, \Gamma(\epsilon_R)) \geq Q(U_L)$. That is, U_R is UC, $Q(U_R)$ is not greater than $Q(U_L)$, but the capacity at ϵ_R is not smaller than $Q(U_L)$. The Riemann problem is solved by a combination of a standing wave and a forward traveling rarefaction wave, with an intermediate state U_1 as shown by the four figures of Figure

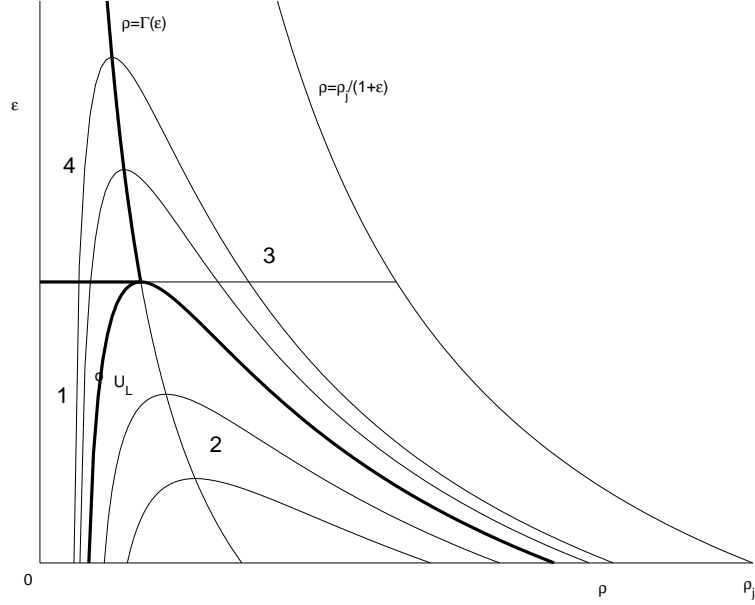


Figure 6: Four types of Riemann solutions when U_L is UC

7. The top left figure in the $\rho - \epsilon$ phase plane shows that (U_L, U_1) is a standing wave, and the two states share the same flow-rate $Q(U_L)$. The bottom left figure shows two fundamental diagrams for when $\epsilon = \epsilon_L$ and $\epsilon = \epsilon_R$ respectively and the Riemann solution of a standing wave and a rarefaction wave. The top right figure shows characteristic waves in the $x - t$ plane, and we can see the discontinuity caused by the standing wave at $x = 0$ and the rarefaction wave on its right side. The bottom right figure shows the profile of density at a time instant t_0 . In this case, since the flow-rate remains the same across $x = 0$, then the boundary flux $q = Q(U_L)$.

As shown in Figure 8, when U_L is OC, i.e. to the right of the transitional curve in the phase plane, we have $\rho_L > \Gamma(\epsilon_L)$ and can divide the $\rho - \epsilon$ phase plane into six regions by the thick curves and obtain the six types of wave solutions for different values of U_R , which satisfy the two aforementioned entropy conditions. The solutions of Types 5 to 10 are also given in Appendix.

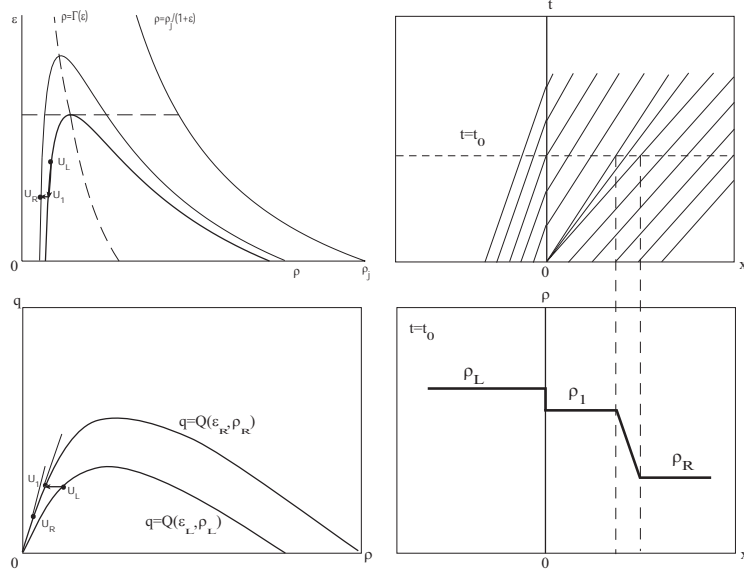


Figure 7: An example for wave solutions to Riemann problem of Type 1

If we introduce new definitions of local traffic supply and demand (Daganzo, 1995; Lebacque, 1996; Nelson and Kumar, 2004) as follows,

$$\begin{aligned}
 S(\epsilon, \rho) &= \max\{Q(\epsilon, \bar{\rho}) : \rho \leq \bar{\rho} \leq \rho_j\}, \\
 D(\epsilon, \rho) &= \max\{Q(\epsilon, \bar{\rho}) : 0 \leq \bar{\rho} \leq \rho\}.
 \end{aligned} \tag{20}$$

This is equivalent to saying that

$$S(\epsilon, \rho) = \begin{cases} Q(\epsilon, \Gamma(\epsilon)), & \rho \in [0, \Gamma(\epsilon)], \\ Q(\epsilon, \rho), & \rho \in (\Gamma(\epsilon), \rho_j]; \end{cases}$$

and

$$D(\epsilon, \rho) = \begin{cases} Q(\epsilon, \rho), & \rho \in [0, \Gamma(\epsilon)], \\ Q(\epsilon, \Gamma(\epsilon)), & \rho \in (\Gamma(\epsilon), \rho_j], \end{cases}$$

where $Q(\epsilon, \Gamma(\epsilon))$ is the capacity at ϵ . These definitions lead to that both local supply and demand are not smaller than flow-rate; i.e., $S(\epsilon, \rho) \geq Q(\epsilon, \rho)$, and $D(\epsilon, \rho) \geq Q(\epsilon, \rho)$.

Type	U_L	$D(U_L)$	U_R	$S(U_R)$	q
1	UC	$Q(U_L)$	UC, $Q(U_R) \leq Q(U_L) \leq Q(\epsilon_R, \Gamma(\epsilon_R))$	$Q(\epsilon_R, \Gamma(\epsilon_R))$	$Q(U_L)$
2			$Q(U_R) > Q(U_L)$	$\geq Q(U_R)$	$Q(U_L)$
3			OC, $Q(U_R) \leq Q(U_L)$	$Q(U_R)$	$Q(U_R)$
4			UC, $Q(\epsilon_R, \Gamma(\epsilon_R)) < Q(U_L)$	$Q(\epsilon_R, \Gamma(\epsilon_R))$	$Q(\epsilon_R, \Gamma(\epsilon_R))$
5	OC	$Q(\epsilon_L, \Gamma(\epsilon_L))$ $\geq Q(U_L)$	OC, $Q(U_R) \leq Q(U_L)$	$Q(U_R)$	$Q(U_R)$
6			OC, $Q(U_L) < Q(U_R) \leq Q(\epsilon_L, \Gamma(\epsilon_L))$	$Q(U_R)$	$Q(U_R)$
7			UC, $Q(U_R) \leq Q(\epsilon_L, \Gamma(\epsilon_L)) \leq Q(\epsilon_R, \Gamma(\epsilon_R))$	$Q(\epsilon_R, \Gamma(\epsilon_R))$	$Q(\epsilon_L, \Gamma(\epsilon_L))$
8			$Q(U_R) > Q(\epsilon_L, \Gamma(\epsilon_L))$	$\geq Q(U_R)$	$Q(\epsilon_L, \Gamma(\epsilon_L))$
9			UC, $Q(\epsilon_R, \Gamma(\epsilon_R)) < Q(U_L)$	$Q(\epsilon_R, \Gamma(\epsilon_R))$	$Q(\epsilon_R, \Gamma(\epsilon_R))$
10			UC, $Q(U_L) \leq Q(\epsilon_R, \Gamma(\epsilon_R)) < Q(\epsilon_L, \Gamma(\epsilon_L))$	$Q(\epsilon_R, \Gamma(\epsilon_R))$	$Q(\epsilon_R, \Gamma(\epsilon_R))$

Table 1: Boundary flux, downstream supply, and upstream demand for ten types of Riemann problems

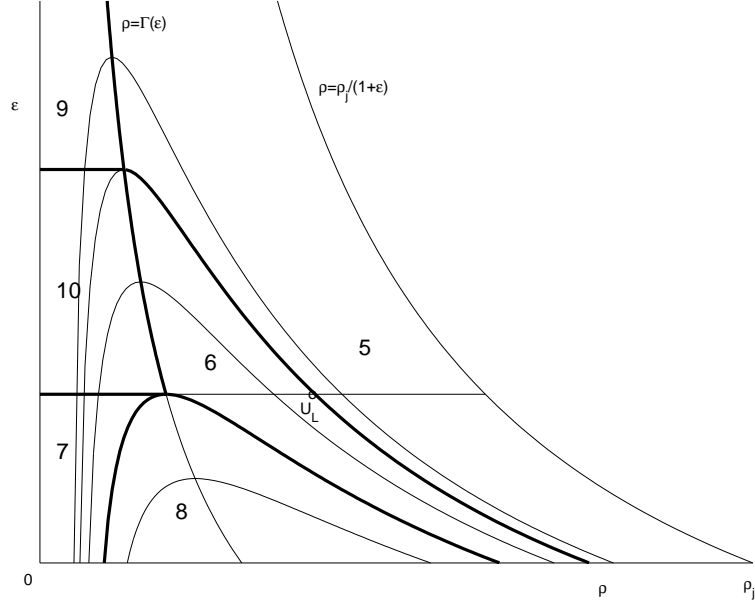


Figure 8: Six types of Riemann solutions when U_L is OC

In **Table 1**, we summarize the solutions of boundary flux for ten types of Riemann problems discussed in the preceding subsection and compute the corresponding upstream demand and downstream supply functions. From the table, we can conclude that the boundary flux can be computed by the minimum of upstream demand and downstream supply; i.e.,

$$q = \min\{S(U_R), D(U_L)\}. \quad (21)$$

Although (21) is proved for time-independent and differential fundamental diagram, we expect that the supply-demand definitions in (20) can also be applied to the triangular fundamental diagram and to the scenarios when ϵ is time-varying. Therefore, this method can be considered as a simplification and extension to the Riemann solver in the preceding subsection and is more efficient for numerical simulations.

4 Calibration of lane-changing intensity in a weaving section

In this section, we consider lane-changing traffic on a multi-lane freeway section on interstate 80 in Emeryville (San Francisco), California, as shown in Figure 9. The freeway section has six lanes, where lane 1 is a car-pool lane, and an on-ramp from Powell Street and an off-ramp to Ashby Ave. The width of lanes 1 to 6 is 12 ft. Traffic direction is from south to north. The road section is covered by seven cameras, numbered 1 to 7 from south to north, and vehicle trajectories were transcribed from video data by FHWA’s NGSIM project (Federal Highway Administration, 2006). In total there are four data sets (Cambridge Systematics, Inc., 2004, 2005a,b,c): Data set 1 contains trajectories of all vehicles every fifteenth second on December 3, 2003 between 2:35pm and 3:05pm; Data sets 2 to 4 contain the locations of each vehicle every tenth second on April 13, 2005 between 4pm and 4:15pm, between 5pm and 5:15pm, and between 5:15pm and 5:30pm, respectively. Note that the lengths of the study location in the first and the other three data sets are different: The Ashby Ave off-ramp is included in the first data set, but not in the other three.

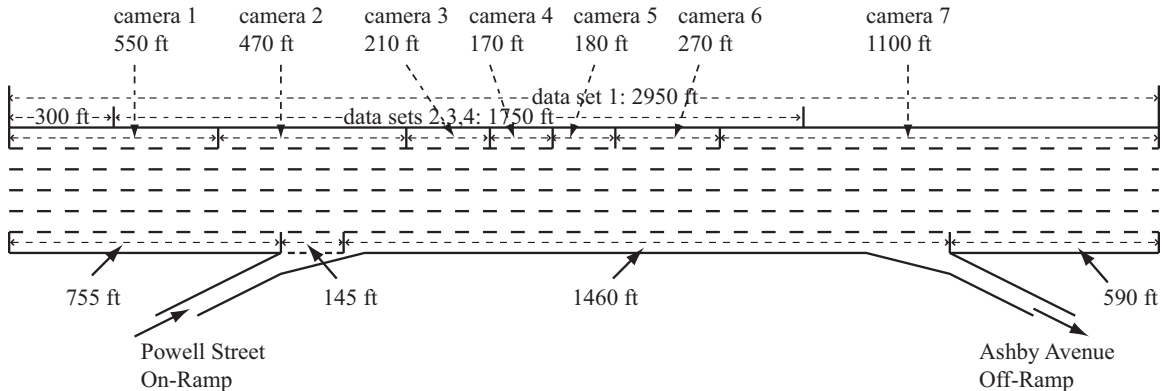


Figure 9: I-80 study area

In Figure 10, we demonstrate the trajectories in both $x-y$ and $t-y$ spaces of vehicle 576 in data set 2, when it switches from lane 6 to lane 5. Here $y = 60$ is the lane separation line, and the width

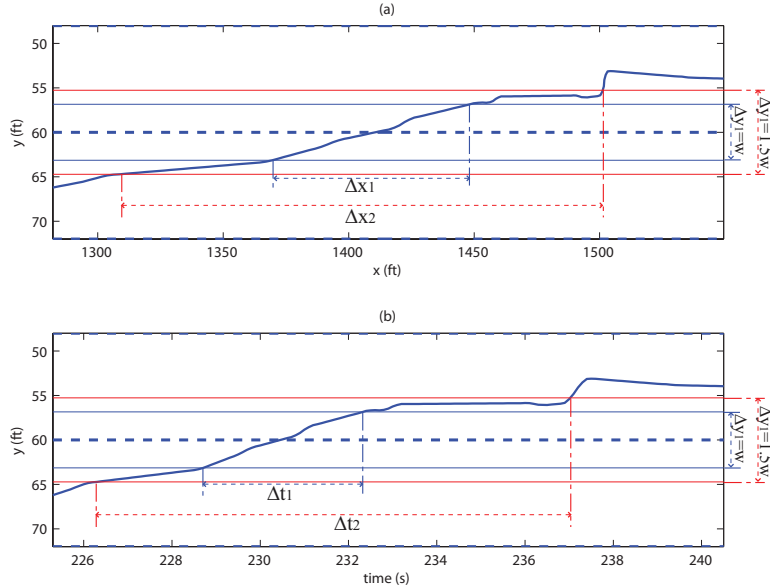


Figure 10: Trajectories of a lane-changing vehicle: (a) in $x - y$ space; (b) in $t - y$ space

of the vehicle is $w = 6.3$ ft. In both figures, we demonstrate Δx and Δt for two different Δy , w or $1.5w$. From both figures, we can see that the lane-changing angles is decreased by more than half and the lane-changing time is more than doubled when we increase Δy from w to $1.5w$. Note that $1.5w$ is still smaller than the width of a lane, 12 ft. From the figures, we can see that, after entering the target lane, the vehicle first stay near the lane separation line and then adjust to the center. Such behavior can be confirmed with video data by camera 6.

Following the example in Section 2.2, we can theoretically derive the lane-changing intensity variable in (12) and corresponding fundamental diagrams in (8) and (7) for a lane-changing area with a width of $L = x_b - x_a$ and time period with a duration of $T = t_b - t_a$, shown in Figure 9. Assume that all lane-changes are induced by on-ramp vehicles and finished in a region of L downstream to the merge and that traffic flow is uniform with speed v and flow-rate q , respectively. Following the example in Section 2.2, we can estimate the number of lane-changes in L during $T = L/v$ as

$2.5q_{on}T$, since one sixth of the on-ramp vehicles will make zero up to five lane-changes. Thus the lane-changing intensity variable can be estimated as

$$\epsilon = \frac{N_{LC}t_{LC}}{\rho LT} = \frac{2.5q_{on}Tt_{LC}}{\rho LT} = 2.5q_{on} \frac{t_{LC}}{\rho L}. \quad (22)$$

Since q_{on} is usually controlled by ramp meters and t_{LC} is almost constant, ϵ is generally not a constant in ρ or v : it is decreasing in ρ and increasing in v , when traffic is congested. In particular, if $q_{on} = 800$ vph, $\rho = 200$ vpm, $L = 900$ ft, and $t_{LC} = 5$ s, we have $\epsilon = 8.15\%$ for $v = 60$ mph. Note that (22) is just an estimation for the weaving region in Figure 9, since (1) lane-changes can also be caused by vehicles leaving to the off-ramp or vehicles from or to other adjacent on- and off-ramps, (2) lane-changes induced by the on-ramp vehicles can occur upstream to the merge, and (3) fewer than one-sixth of the on-ramp vehicles can make five lane-changes, since the first lane is a car-pool lane.

In the following, we consider a road section of 900 ft downstream to the merge in Figure 9 with $x_a = 950$ ft and $x_b = 1850$ ft. The length is $L = 900$ ft or 274 m. The time interval is $[t_i, t_i + T]$, where the smallest t_i is the time when the first vehicles pass x_b , and the greatest $t_i + T$ is the time when the last vehicles pass x_a . For four data sets, $T = 39, 63, 86, 100$ s, respectively. Here we consider different lane-changing thresholds Δy . Refer to (Jin, 2010) for detailed methods for computing θ , ϵ , ρ , q , and v .

With a lane-changing threshold of $\Delta y = w$, we have the following results. From Figure 11, we find a linear relationship between density and lane-changing angle

$$\theta = -0.5016 + 0.0121\rho,$$

with R-square 0.9441. Here we can also calibrate a relationship similar to (22) as

$$\epsilon = -0.0247 + \frac{24.2712}{\rho},$$

with R-square 0.8077. Hereafter we only calibrate the exponential function, since it usually yields better R-square. From Figure 12, we can see that $q = \rho V(\rho)$ has a capacity of 13408 mph when $\rho = 233$ vpm, and $q = \rho V((1 + \epsilon)\rho)$ has a capacity of 12369 mph when $\rho = 215$ vpm. Lane-changes can cause 7.75% reduction in capacity.

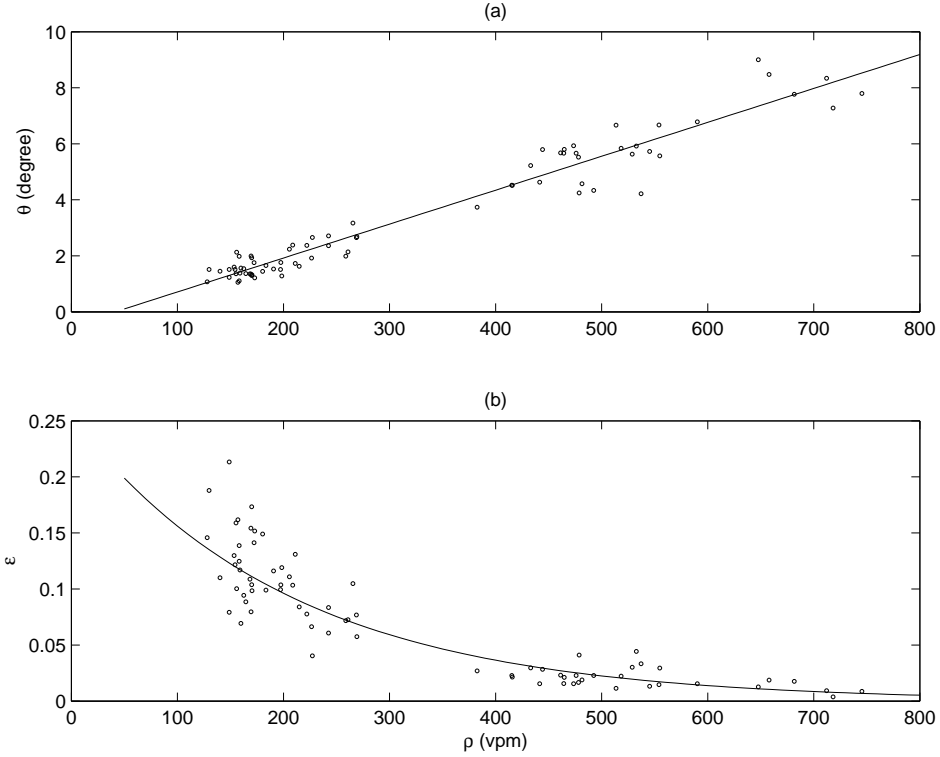


Figure 11: Characteristics of lane-changes at different densities with a threshold of w

With a lane-changing threshold of $\Delta y = 1.5w$, from Figure 13, we find a linear relationship between density and lane-changing angle

$$\theta = -0.3222 + 0.0086\rho,$$

with R-square 0.9139. We can also find the following relationship between density and ϵ

$$\epsilon = 0.5579e^{-0.0048\rho},$$

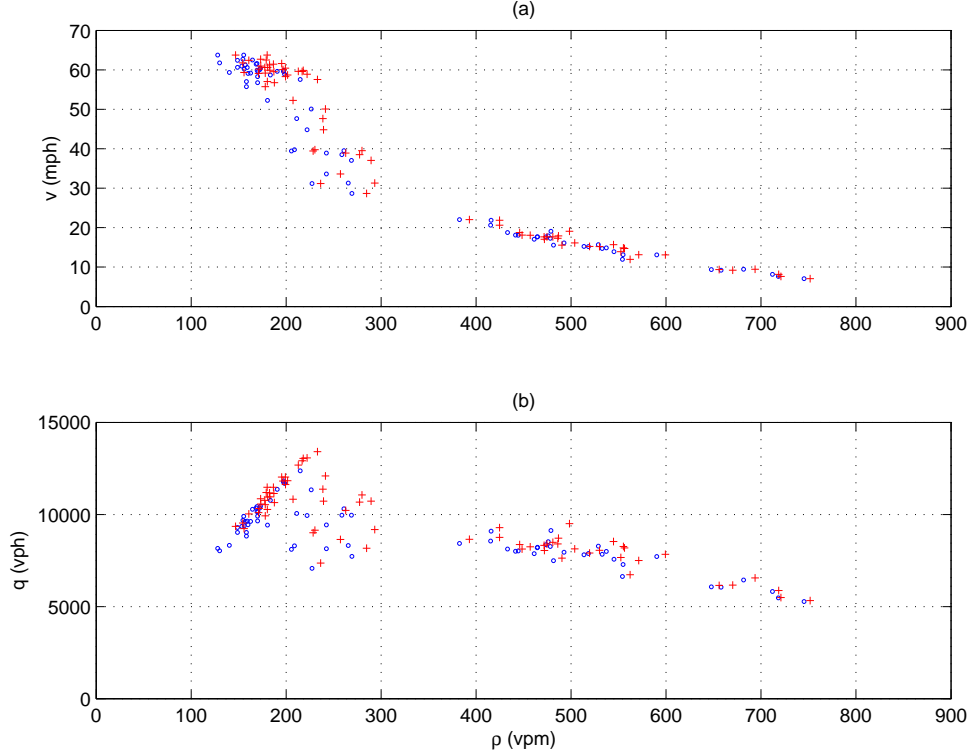


Figure 12: Fundamental diagrams with a threshold of w : Blue dots with lane-changing effect, and red dots without lane-changing effect

with R-square 0.8917. From Figure 14, we can see that $q = \rho V(\rho)$ has a capacity of 15014 mph when $\rho = 251$ vpm, and $q = \rho V((1 + \epsilon)\rho)$ has a capacity of 12369 mph when $\rho = 215$ vpm. The lane-changes cause 17.62% capacity reduction. Potential capacity drop is more than twice than that for $\Delta y = w$. This is consistent with the observation in Figure 10, since t_{LC} is more than doubled with $\Delta y = 1.5w$.

For the whole weaving location, we have density-dependent lane-changing intensity variables. More detailed analysis show that ϵ is also location-dependent (Jin, 2010). Note that the kinematic wave model (9) is developed for a roadway with both lane-changing and normal sections. If we can

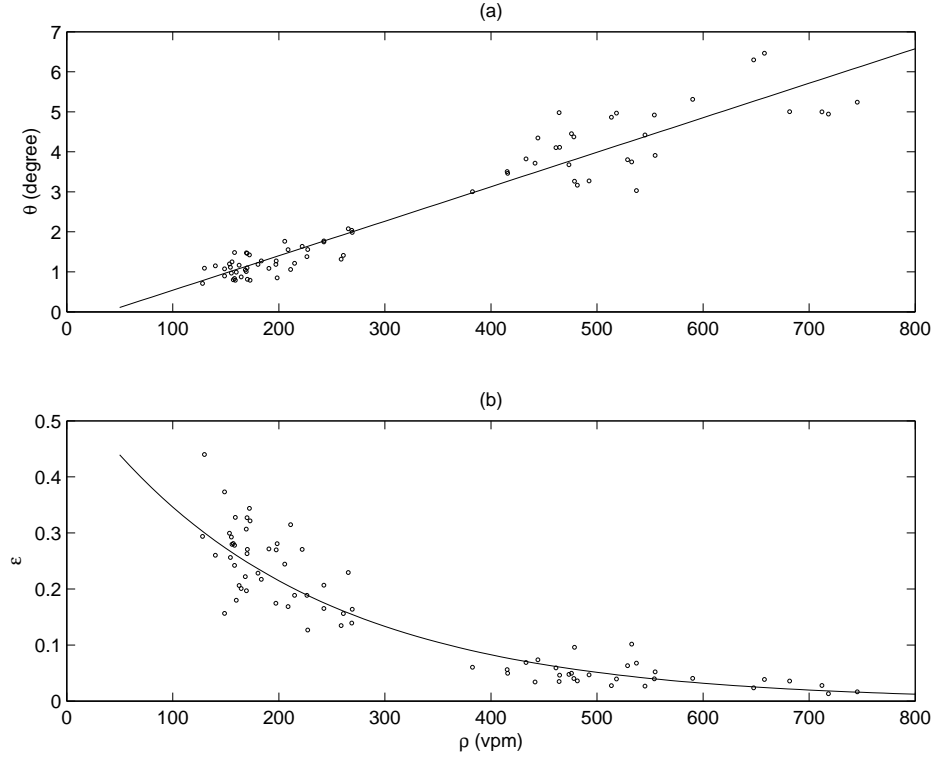


Figure 13: Characteristics of lane-changes at different densities with a threshold of $\frac{3}{2}w$

obtain an $\epsilon - \rho$ relation everywhere, (9) can be re-written as

$$\rho_t + (\rho V(\rho(1 + \epsilon(x, \rho))))_x = 0. \quad (23)$$

If we define $Q(x, \rho) = \rho V(\rho(1 + \epsilon(x, \rho)))$, this model is equivalent to an inhomogeneous LWR model.

In this case, if we are able to introduce an inhomogeneity factor and write the equation above as a system of hyperbolic conservation laws, the analysis in Section 3 will apply for this general model.

When we are not able to introduce an inhomogeneity factor, we can use the supply-demand method in (21) for numerical solutions of the kinematic wave model of lane-changing traffic (9).

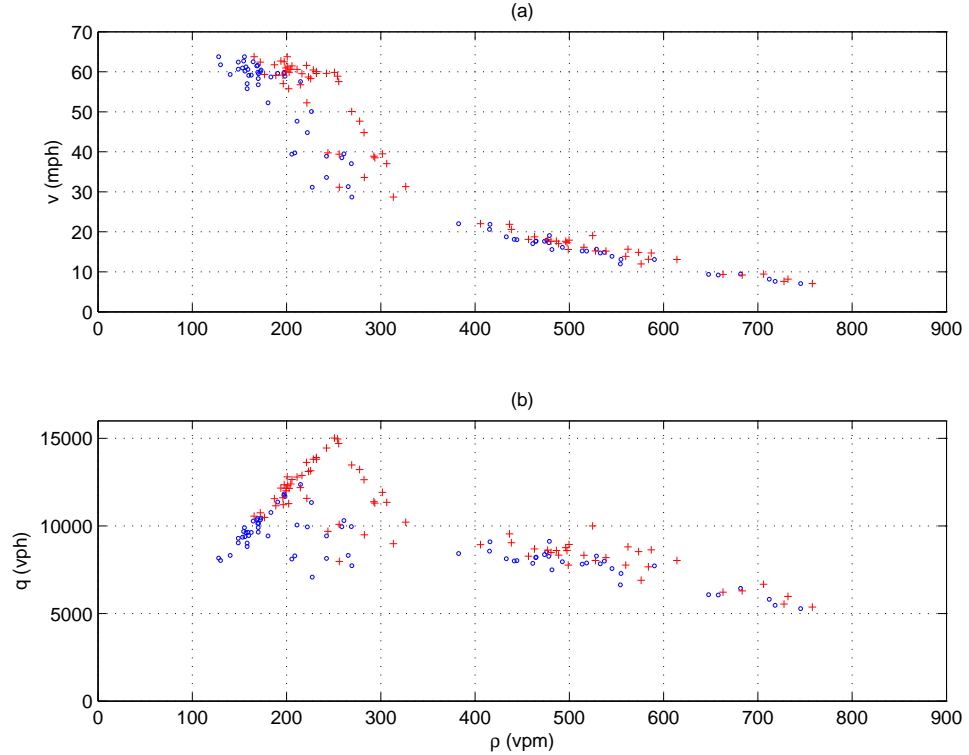


Figure 14: Fundamental diagrams with a threshold of $\frac{3}{2}w$: Blue dots with lane-changing effect, and red dots without lane-changing effect

5 Conclusion

In this paper, we presented a model for lane-changing traffic dynamics in the framework of kinematic waves. A key assumption is that the disruption lane-changing effect can be modeled by a modified speed-density relation with a new lane-changing intensity variable. Then, for location-dependent lane-changing intensities, we studies kinematic waves arising in lane-changing traffic and corresponding new definitions of local traffic supply and demand for computing the flow passing through a boundary. With both theoretical derivations and observed data, we demonstrated that lane-changing intensities are highly related to road geometry, location, on-ramp/off-ramp traffic,

lane-changing time, vehicle speeds, and other traffic conditions. In particular, with 75 minutes of vehicle trajectories collected for a freeway section on interstate 80, we calibrated lane-changing intensities and corresponding fundamental diagrams for different lane-changing thresholds. The results support a functional relationship between density and the lane-changing effect for the whole weaving section, and the lane-changing angles are highly related to traffic density. Furthermore, it was suggested that lane-changes could cause 8% to 18% reduction in capacity, depending on the definition of a lane-changing threshold.

By incorporating lane-changing effects in the fundamental diagram, this study provides a simple framework to look into lane-changing traffic dynamics in the framework of kinematic wave theory. From this study, we can see that lane-changing traffic could cause capacity drop, different observed jam densities, and fundamental diagram of reverse- λ shape. Lane-changing traffic can also affect the formation and dissipation of shock and rarefaction waves on a roadway. This simple model can be easily integrated into a commodity-based kinematic wave simulation model of network traffic in (Jin and Zhang, 2004; Jin and Jayakrishnan, 2005) to study system-wide traffic dynamics.

The model studied here bears certain limitations by assuming full balance among lanes and constant ϵ . Thus our model is not intended for ramp weaves (HCM 2000), but for usually balanced areas near a lane-drop or merging junction. By assuming an equilibrium speed-density relationship, (9) is not able to describe detailed traffic dynamics when vehicles are accelerating or decelerating. In this study, we only studied the bottleneck effects of lane-changing traffic. In relatively sparse traffic, however, lane-changes could actually benefit the overall traffic flow due to their balancing effects, and such effects have yet to be included in ϵ . In addition, the new model considers the lateral interactions between vehicles in lane-changing areas at the aggregate level, and more detailed analysis of microscopic lane-changing decisions and maneuvers could give us more insights on the aggregate effects of lane-changing traffic.

With observed data, we calibrated a simple relationship between lane-changing intensity and traffic density. As shown in (22), lane-changing intensity is also related to on-ramp and off-ramp flows. For the weaving section in Figure 9, however, we do not have off-ramp flows in data sets 2 to 4 and therefore cannot study such relationships. In addition, it was shown that Δy could significantly impact lane-changing intensities and therefore capacity reductions, and it can be calibrated by comparing road capacities with lane-changes and those without lane-changes. For example, for the weaving section studied in Section 4, capacity reductions are about 8% and 18% when Δy is set to be a vehicles width and 1.5 times of a vehicles width, respectively. In the future, we will be interested in calibrating the lane-changing threshold with more data sets or more detailed analysis. In the future, we will also be interested in studying lane-changing intensities for different lane-changing areas, on-ramp/off-ramp flows, and other factors. Such a study would be helpful for understanding traffic macroscopic traffic dynamics in lane-changing areas and for developing possible ramp-metering and lane management strategies for improving the overall traffic flow.

Acknowledgments

We would like to thank Dr. Shin-Ting (Cindy) Jeng for her valuable comments and discussions. The comments by several anonymous reviewers have been very helpful for improving the presentation of the paper. The views and results herein are the author's alone.

References

Cambridge Systematics, Inc., September 2004. NGSIM BHL Data Analysis. Tech. rep., summary Report, Prepared for Federal Highway Administration.

- Cambridge Systematics, Inc., September 2005a. NGSIM I-80 Data Analysis (4:00 p.m. to 4:15 p.m.).
Tech. rep., summary Report, Prepared for Federal Highway Administration.
- Cambridge Systematics, Inc., September 2005b. NGSIM I-80 Data Analysis (5:00 p.m. to 5:15 p.m.).
Tech. rep., summary Report, Prepared for Federal Highway Administration.
- Cambridge Systematics, Inc., September 2005c. NGSIM I-80 Data Analysis (5:15 p.m. to 5:30 p.m.).
Tech. rep., summary Report, Prepared for Federal Highway Administration.
- Cassidy, M., Rudjanakanoknad, J., 2005. Increasing the capacity of an isolated merge by metering its on-ramp. *Transportation Research Part B* 39 (10), 896–913.
- Cassidy, M., Skabardonis, A., May, A. D., 1989. Operation of major freeway weaving sections: recent empirical evidence. *Transportation Research Record: Journal of the Transportation Research Board* 1225, 61–72.
- Cassidy, M. J., Bertini, R. L., 1999. Some traffic features at freeway bottlenecks. *Transportation Research Part B* 33 (1), 25–42.
- Cassidy, M. J., May, A. D., 1991. Proposed analytical technique for estimating capacity and level of service of major freeway weaving sections. *Transportation Research Record: Journal of the Transportation Research Board* 1320, 99–109.
- Chang, G.-L., Kao, Y.-M., November 1991. An empirical investigation of macroscopic lane-changing characteristics on uncongested multilane freeways. *Transportation Research Part A* 25 (6), 375–389.
- Coifman, B., 2003. Estimating density and lane inflow on a freeway segment. *Transportation Research Part A* 37 (8), 689–701.

- Daganzo, C. F., 1995. The cell transmission model II: Network traffic. *Transportation Research Part B* 29 (2), 79–93.
- Daganzo, C. F., 2002. A behavioral theory of multi-lane traffic flow. Part I: Long homogeneous freeway sections. II: Merges and the onset of congestion. *Transportation Research Part B* 36, 131–169.
- Del Castillo, J. M., Benitez, F. G., 1995. On the functional form of the speed-density relationship - II: Empirical investigation. *Transportation Research Part B* 29 (5), 391–406.
- Eads, B. S., Roupail, N. M., May, A. M., Hall, F., 2000. Freeway facility methodology in “Highway Capacity Manual” 2000. *Transportation Research Record: Journal of the Transportation Research Board* 1710, 171–180.
- Fazio, J., Roupail, N. M., 1986. Freeway weaving sections: comparison and refinement of design and operations analysis procedures. *Transportation Research Record: Journal of the Transportation Research Board* 1091, 101–109.
- Federal highway administration, 2000. Highway capacity manual. Tech. rep., Transportation Research Board, National Research Council, Washington, D.C.
- Federal Highway Administration, December 2006. Next Generation SIMulation Fact Sheet. Tech. rep., FHWA-HRT-06-135.
- Fitzpatrick, K., Nowlin, L., 1996. One-sided weaving operations on one-way frontage roads. *Transportation Research Record: Journal of the Transportation Research Board* 1555, 42–49.
- Gazis, D. C., Herman, R., Rothery, R. W., 1961. Nonlinear follow-the-leader models of traffic flow. *Operations Research* 9 (4), 545–567.

- Gazis, D. C., Herman, R., Weiss, G. H., 1962. Density oscillations between lanes of a multilane highway. *Operations Research* 10 (5), 658–667.
- Gipps, P. G., 1986. A model for the structure of lane changing decisions. *Transportation Research Part B* 20 (5), 403–414.
- Godunov, S. K., 1959. A difference method for numerical calculations of discontinuous solutions of the equations of hydrodynamics. *Matematicheskii Sbornik* 47, 271–306, in Russian.
- Golob, T. F., Recker, W. W., Alvarez, V. M., January 2004. Safety aspects of freeway weaving sections. *Transportation Research Part A: Policy and Practice* 38 (1), 35–51.
- Greenshields, B. D., 1935. A study in highway capacity. *Highway Research Board Proceedings* 14, 448–477.
- Haberman, R., 1977. *Mathematical models*. Prentice Hall, Englewood Cliffs, NJ.
- Hall, F. L., Agyemang-Duah, K., 1991. Freeway capacity drop and the definition of capacity. *Transportation Research Record: Journal of the Transportation Research Board* 1320, 91–98.
- Holland, E. N., Woods, A. W., November 1997. A continuum model for the dispersion of traffic on two-lane roads. *Transportation Research Part B* 31 (6), 473–485.
- Isaacson, E. I., Temple, J. B., 1992. Nonlinear resonance in systems of conservation laws. *SIAM Journal on Applied Mathematics* 52 (5), 1260–1278.
- Jin, W.-L., 2010. Macroscopic characteristics of lane-changing vehicular traffic. In: *Proceedings of Transportation Research Board Annual Meeting*. To be presented.
- Jin, W.-L., Chen, L., Puckett, E. G., 2009. Supply-demand diagrams and a new framework for analyzing the inhomogeneous Lighthill-Whitham-Richards model. *Proceedings of the 18th International Symposium on Transportation and Traffic Theory (ISTTT18)*, 603–635.

- Jin, W.-L., Jayakrishnan, R., 2005. First-in-first-out properties of a commodity-based kinematic wave simulation model. *Transportation Research Record: Journal of the Transportation Research Board* 1934, 197–207.
- Jin, W.-L., Zhang, H. M., August 2003. The inhomogeneous kinematic wave traffic flow model as a resonant nonlinear system. *Transportation Science* 37 (3), 294–311.
- Jin, W.-L., Zhang, H. M., 2004. A multicommodity kinematic wave simulation model of network traffic flow. *Transportation Research Record: Journal of the Transportation Research Board* 1883, 59–67.
- Jin, W.-L., Zhang, Y., Chu, L., 2006. Measuring first-in-first-out violation among vehicles. In: *Proceedings of Transportation Research Board Annual Meeting*.
- Kesting, A., Treiber, M., Helbing, D., 2007. General Lane-Changing Model MOBIL for Car-Following Models. *Transportation Research Record: Journal of the Transportation Research Board* 1999 (-1), 86–94.
- Klar, A., Wegener, R., 1999. A hierarchy of models for multilane vehicular traffic I: Modeling. II: Numerical investigations. *SIAM Journal on Applied Mathematics* 59 (3), 983–1011.
- Koshi, M., Iwasaki, M., Ohkura, I., 1983. Some findings and an overview on vehicular flow characteristics. In: Hurdle, V. F., Hauer, R., Stewart, G. N. (Eds.), *Proceedings of the Eighth International Symposium on Transportation and Traffic Theory*. University of Toronto Press, Toronto, Ontario, pp. 403–426.
- Laval, J., Daganzo, C., 2006. Lane-changing in traffic streams. *Transportation Research Part B* 40 (3), 251–264.

- Lax, P. D., 1972. Hyperbolic systems of conservation laws and the mathematical theory of shock waves. SIAM, Philadelphia, Pennsylvania.
- Lebacque, J. P., 1996. The Godunov scheme and what it means for first order traffic flow models. In: The International Symposium on Transportation and Traffic Theory. Lyon, France.
- Leisch, J. E., 1979. A new technique for design and analysis of weaving sections on freeways. ITE Journal 49 (3), 26–29.
- Lighthill, M. J., Whitham, G. B., 1955. On kinematic waves: II. A theory of traffic flow on long crowded roads. Proceedings of the Royal Society of London A 229 (1178), 317–345.
- Michalopoulos, P. G., Beskos, D. E., Yamauchi, Y., 1984. Multilane traffic flow dynamics: Some macroscopic considerations. Transportation Research Part B 18 (4/5), 377–395.
- Milam, R. T., Choa, F., 1998. A comparison of partial and full partial cloverleaf interchange operations using the CORSIM micro-simulation model. In: ITE District 6 Annual Conference. San Jose, California.
- Munjal, P. K., Hsu, Y. S., Lawrence, R. L., 1971. Analysis and validation of lane-drop effects of multilane freeways. Transportation Research 5, 257–266.
- Munjal, P. K., Pipes, L. A., 1971. Propagation of on-ramp density waves on uniform unidirectional multilane freeways. Transportation Research 5, 241–255.
- Nelson, P., Kumar, N., 2004. Point constriction, interface and boundary conditions for the kinematic-wave model. In: Proceedings of Transportation Research Board Annual Meeting.
- Newell, G. F., 1961. Nonlinear effects in the dynamics of car following. Operations Research 9 (2), 209.

- Newell, G. F., 1993. A simplified theory of kinematic waves in highway traffic I: General theory. II: Queuing at freeway bottlenecks. III: Multi-destination flows. *Transportation Research Part B* 27 (4), 281–313.
- Ostrom, B., Leiman, L., May, A. D., 1993. Suggested procedures for analyzing freeway weaving sections. *Transportation Research Record: Journal of the Transportation Research Board* 1398, 42–48.
- Pahl, J., 1972. Lane-change frequencies in freeway traffic flow. *Highway Research Record* 409, 17–25.
- Richards, P. I., 1956. Shock waves on the highway. *Operations Research* 4, 42–51.
- Roess, R. P., McShane, W. R., Pignataro, L. J., 1974. Configuration, design, and analysis of weaving sections. *Transportation Research Record: Journal of the Transportation Research Board* 489, 1–12.
- Sheu, J.-B., Ritchie, S. G., 2001. Stochastic modeling and real-time prediction of vehicular lane-changing behavior. *Transportation Research Part B* 35 (7), 695–716.
- Toledo, T., Koutsopoulos, H. N., Ben-Akiva, M. E., 2003. Modeling integrated lane-changing behavior. In: *Proceedings of Transportation Research Board Annual Meeting*.
- Wang, Y., Prevedouros, P. D., 1998. Comparison of INTEGRATION, TSIS/CORSIM and WATSim in replicating volumes and speeds on three small networks. *Transportation Research Record: Journal of the Transportation Research Board* 1644, 80–92.
- Whitham, G. B., 1974. *Linear and nonlinear waves*. John Wiley and Sons, New York.
- Windover, J. R., May, A. D., 1994. Revisions to level D methodology of analyzing freeway ramp weaving sections. *Transportation Research Record: Journal of the Transportation Research Board* 1457, 43–49.

Worrall, R. D., Bullen, A. G. R., 1970. An empirical lane-changing model on multilane highways. Highway Research Record 303, 30–43.

Worrall, R. D., Bullen, A. G. R., Gur, Y., 1970. An elementary stochastic model of lane-changing on a multilane highway. Highway Research Record 308, 1–12.

Yang, Q., 1997. A simulation laboratory for evaluation of dynamic traffic management systems. Ph.D. thesis, Massachusetts Institute of Technology, Cambridge, Massachusetts.

Appendix: Kinematic wave solutions of Types 2 to 10

Type 2 When U_R is in Region 2, $Q(U_R) > Q(U_L)$. The Riemann problem is solved by a combination of a standing wave and a forward traveling shock wave, with an intermediate state U_1 as shown in Figure 15. In this case, $q = Q(U_L)$.

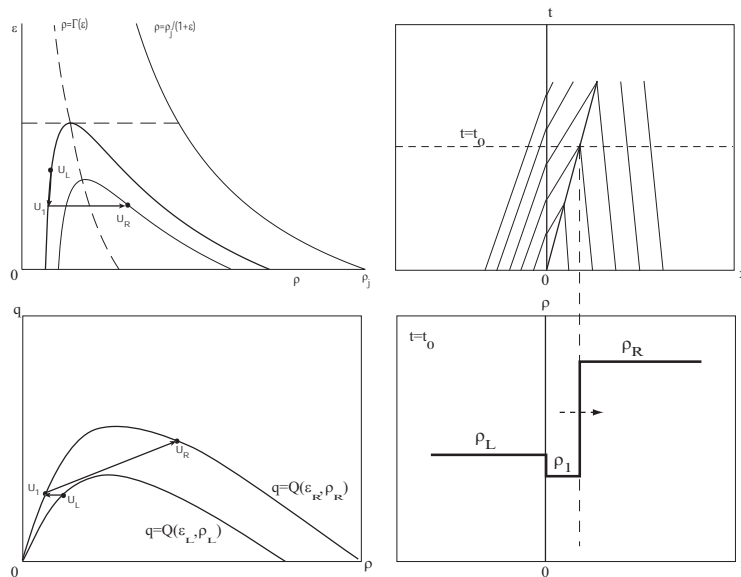


Figure 15: An example for wave solutions to Riemann problem of Type 2

Type 3 When U_R is in Region 3, $\rho_R > \Gamma(\epsilon_R)$ and $Q(U_R) \leq Q(U_L)$. That is, U_R is OC, and $Q(U_R)$ is not greater than $Q(U_L)$. The Riemann problem is solved by a combination of a backward traveling shock wave and a standing wave, with an intermediate state U_1 as shown in Figure 16. In this case, $q = Q(U_R)$.

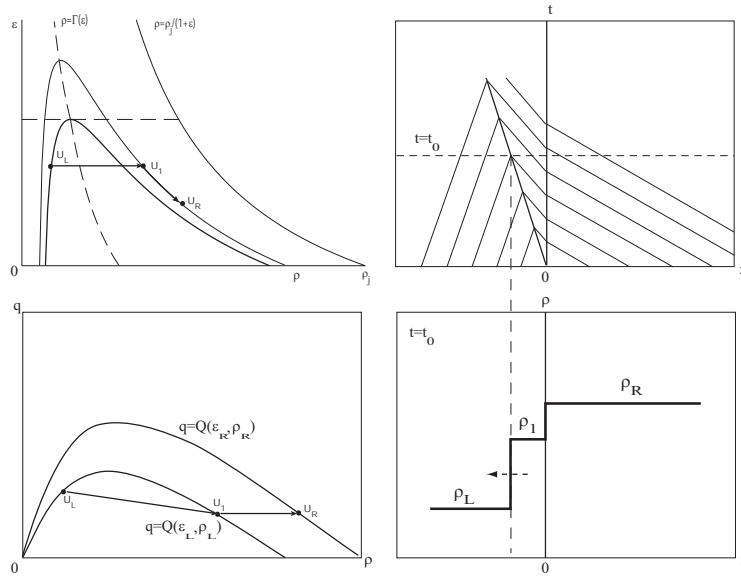


Figure 16: An example for wave solutions to Riemann problem of Type 3

Type 4 When U_R is in Region 4, $\rho_R \leq \Gamma(\epsilon_R)$, $Q(U_R) \leq Q(U_L)$, and $Q(\epsilon_R, \Gamma(\epsilon_R)) < Q(U_L)$. That is, U_R is UC, and the capacity at ϵ_R is smaller than $Q(U_L)$. The Riemann problem is solved by a combination of a backward traveling shock wave, a standing wave, and a forward traveling rarefaction wave, with two intermediate states U_1 and U_2 as shown in Figure 17, where $U_2 = (\epsilon_R, \Gamma(\epsilon_R))$. In this case, $q = Q(\epsilon_R, \Gamma(\epsilon_R))$, which is the capacity flow associated with ϵ_R .

Type 5 When U_R is in Region 5, $\rho_R \geq \Gamma(\epsilon_R)$ and $Q(U_R) \leq Q(U_L)$. That is, U_R is OC, and $Q(U_R)$ is not greater than $Q(U_L)$. The Riemann problem is solved by a combination of a backward traveling shock wave and a standing wave, with an intermediate state U_1 as shown in Figure

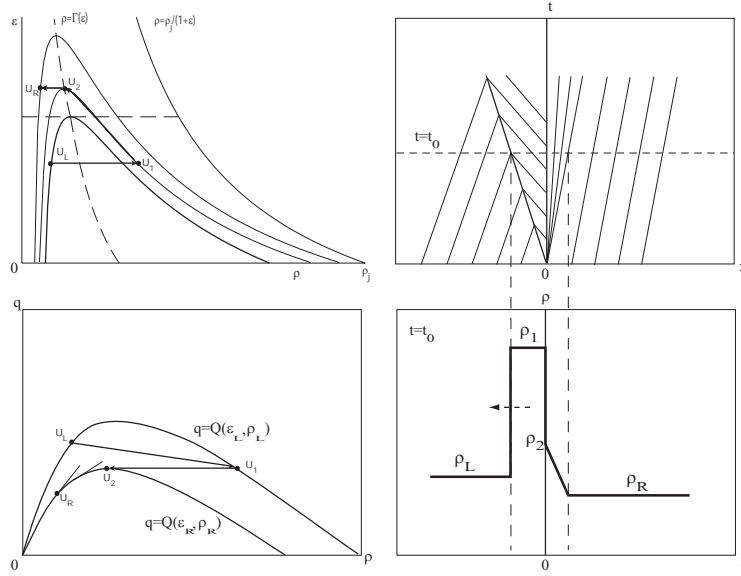


Figure 17: An example for wave solutions to Riemann problem of Type 4

18. In this case, $q = Q(U_R)$.

Type 6 When U_R is in Region 6, $\rho_R \geq \Gamma(\epsilon_R)$ and $Q(U_L) < Q(U_R) \leq Q(\epsilon_L, \Gamma(\epsilon_L))$. That is, U_R is OC, and $Q(U_R)$ is between $Q(U_L)$ and the capacity at ϵ_L . The Riemann problem is solved by a combination of a backward traveling rarefaction wave and a standing wave, with an intermediate state U_1 as shown in Figure 19. In this case, $q = Q(U_R)$.

Type 7 When U_R is in Region 7, $\rho_R < \Gamma(\epsilon_R)$, $Q(U_R) \leq Q(\epsilon_L, \Gamma(\epsilon_L))$, but $Q(\epsilon_R, \Gamma(\epsilon_R)) \geq Q(\epsilon_L, \Gamma(\epsilon_L))$. That is, U_R is UC, and the capacity at ϵ_L is between $Q(U_R)$ and the capacity at ϵ_R . The Riemann problem is solved by a combination of a backward traveling rarefaction wave, a standing wave, and a forward traveling rarefaction wave, with two intermediate state U_1 and U_2 as shown in Figure 20, where $U_1 = (\epsilon_L, \Gamma(\epsilon_L))$. In this case, $q = Q(U_2) = Q(U_1) = Q(\epsilon_L, \Gamma(\epsilon_L))$, the capacity flow when $\epsilon = \epsilon_L$.

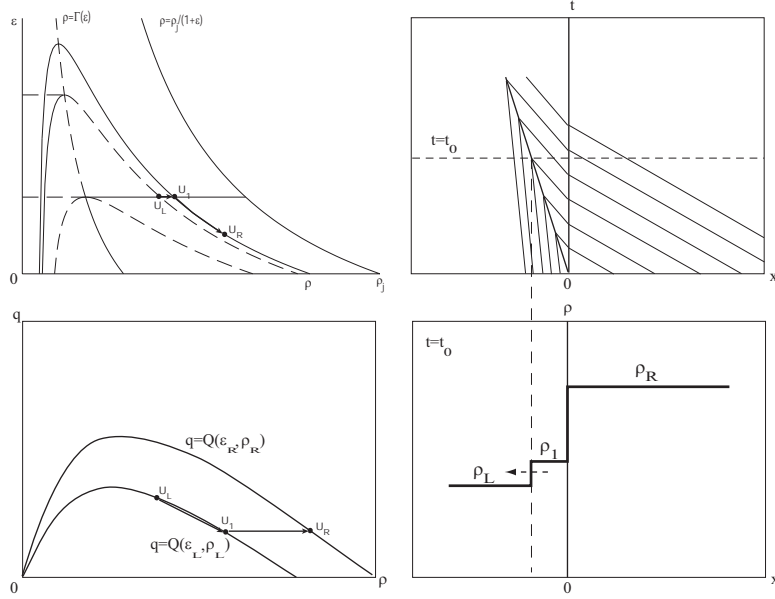


Figure 18: An example for wave solutions to Riemann problem of Type 5

Type 8 When U_R is in Region 8, $Q(U_R) > Q(\epsilon_L, \Gamma(\epsilon_L))$. The Riemann problem is solved by a combination of a backward traveling rarefaction wave, a standing wave, and a forward traveling shock wave, with two intermediate state U_1 and U_2 as shown in Figure 21, where $U_1 = (\epsilon_L, \Gamma(\epsilon_L))$. In this case, $q = Q(U_2) = Q(U_1) = Q(\epsilon_L, \Gamma(\epsilon_L))$.

Type 9 When U_R is in Region 9, $\rho_R < \Gamma(\epsilon_R)$, $Q(U_R) < Q(U_L)$, and $Q(\epsilon_R, \Gamma(\epsilon_R)) < Q(U_L)$. That is, U_R is UC, and both $Q(U_R)$ and the capacity at ϵ_R are smaller than $Q(U_L)$. The Riemann problem is solved by a combination of a backward traveling shock wave, a standing wave, and a forward traveling rarefaction wave, with two intermediate state U_1 and U_2 as shown in Figure 22, where $U_2 = (\epsilon_R, \Gamma(\epsilon_R))$. In this case, $q = Q(U_1) = Q(U_2) = Q(\epsilon_R, \Gamma(\epsilon_R))$.

Type 10 When U_R is in Region 10, $\rho_R < \Gamma(\epsilon_R)$, and $Q(U_L) \leq Q(\epsilon_R, \Gamma(\epsilon_R)) < Q(\epsilon_L, \Gamma(\rho_L))$. That is, U_R is UC, and the capacity at ϵ_R is between $Q(U_L)$ and the capacity at ϵ_L . The Riemann problem is solved by a combination of a backward traveling rarefaction wave, a standing wave,

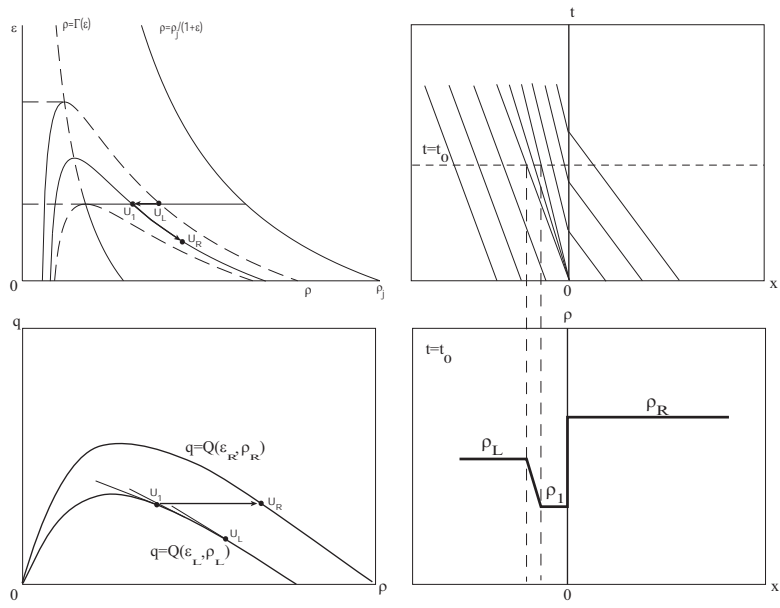


Figure 19: An example for wave solutions to Riemann problem of Type 6

and a forward traveling rarefaction wave, with two intermediate state U_1 and U_2 as shown in Figure 23, where $U_2 = (\epsilon_R, \Gamma(\epsilon_R))$. In this case, $q = Q(U_1) = Q(U_2) = Q(\epsilon_R, \Gamma(\epsilon_R))$.

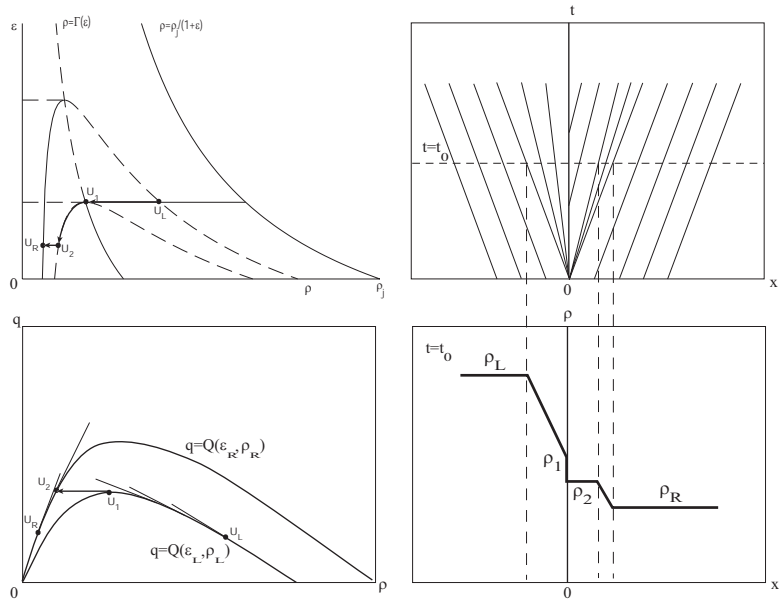


Figure 20: An example for wave solutions to Riemann problem of Type 7

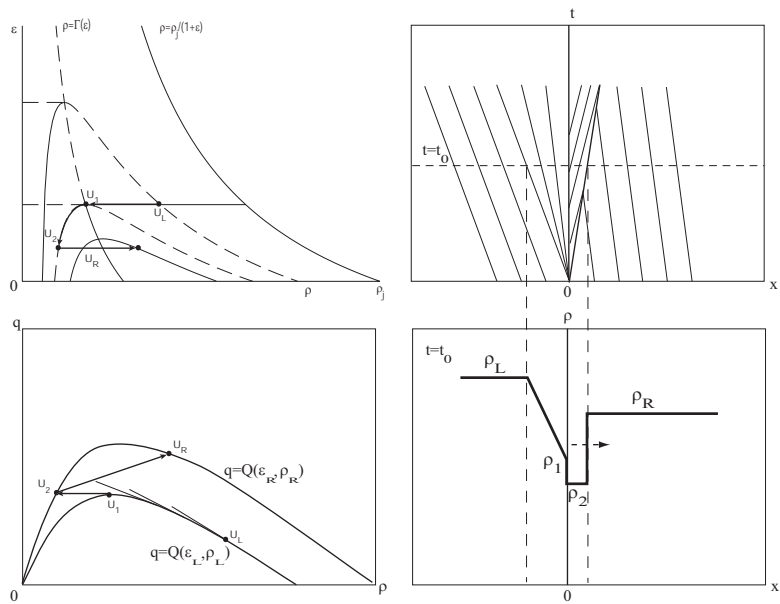


Figure 21: An example for wave solutions to Riemann problem of Type 8

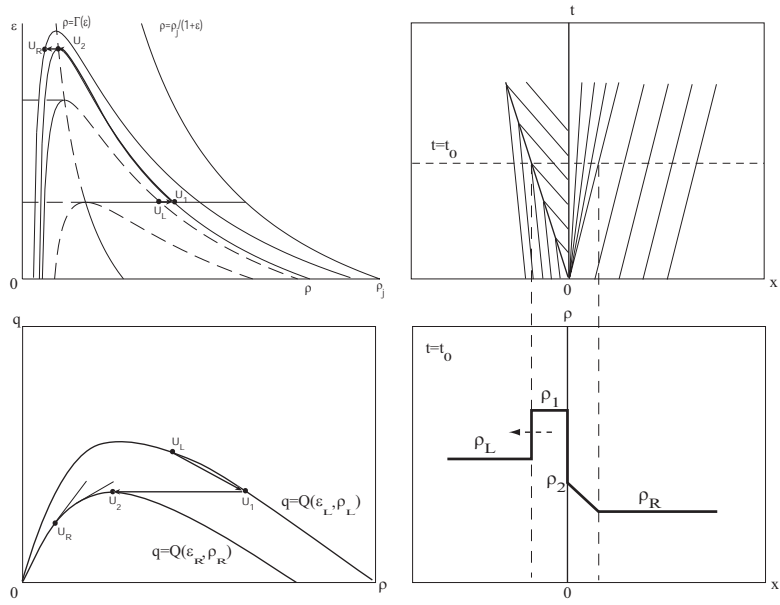


Figure 22: An example for wave solutions to Riemann problem of Type 9

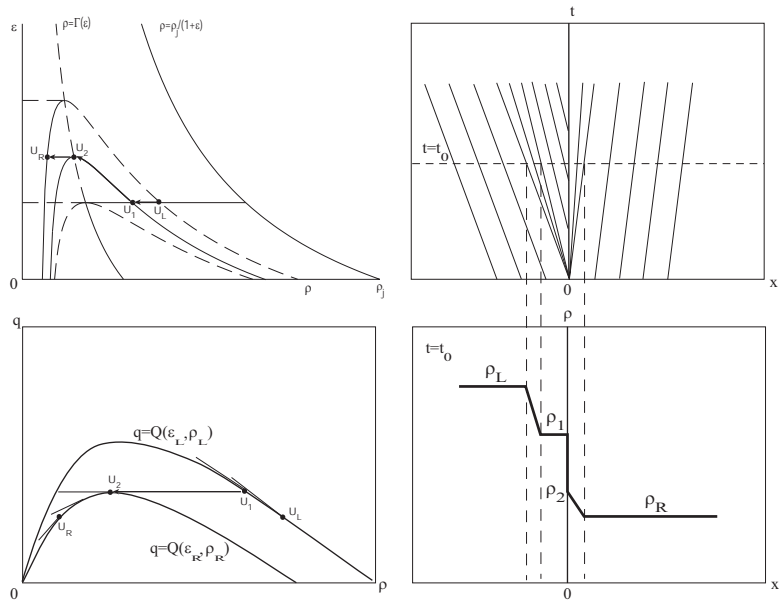


Figure 23: An example for wave solutions to Riemann problem of Type 10